JOURNAL OF GEOPHYSICAL RESEARCH, VOL. 99, NO. C10, PAGES 20,403–20,416, OCTOBER 15, 1994

Surface heat flux, horizontal advection, and the seasonal evolution of water temperature on the Scotian Shelf

Joseph U. Umoh and Keith R. Thompson
Department of Oceanography, Dalhousie University, Halifax, Nova Scotia, Canada

Abstract. Seasonal temperature variations on the Scotian Shelf penetrate to a depth of about 75 m. The net surface heat flux (Q) can explain about 85% of the annual cycle in the rate of change of mean temperature over this depth range. The long-term mean heat budget for a midshelf location shows that horizontal advection (-40 W m^{-2}) is almost exactly balanced by the combined contributions of Q (25 W m^{-2}), horizontal mixing (11 W m^{-2}), and vertical diffusion (6 W m^{-2}). The seasonal evolution of temperature structure on the mid-Scotian Shelf is modeled with a one-dimensional vertical diffusion equation, modified to include the effect of horizontal advection. The model features a vertical eddy diffusivity (K_v) that varies with the background density stratification (N) according to the parameterization $K_v = K_0(1 + \alpha N^p)^{-1}$. The three free parameters (K_0, α and p) are estimated by best fitting, in a least squares sense, the predicted temperatures to observations at standard depths between the surface and 100 m. Typical values of K_v lie in the range 0.2–20 $\times$ 10^{-4} m^2 s^{-1} with the highest values found in winter and close to the surface, as expected. The root mean square of the differences between observed and predicted monthly temperatures is small and equal to 1.0°C. The root mean square of the errors increases significantly (from 1.0°C to 3.1°C) on fitting with a constant K_v, highlighting the importance of allowing K_v to vary with depth and time. The diffusion model is finally used to examine the role of Q and horizontal advection in the seasonal evolution of the temperature profile on the Scotian Shelf and, in particular, the cold intermediate layer which is a prominent feature of the hydrography on the midshelf.

1. Introduction

The northwest Atlantic exhibits the strongest sea surface temperature (SST) variability of any region in the Atlantic between 30°S and 70°N [*Weare*, 1977]. The seasonal cycle has a range of about 16°C (Figure 1). The monthly variations about this seasonal cycle are also large and, at times, have exceeded 5°C. For example, from the early 1950s to the mid 1960s, the SST on the Scotian Shelf dropped by about 5°C, a large change even in comparison to those predicted recently under doubling CO_2 climate scenarios. To fit this variability into a more global perspective, note that the standard deviation of the monthly anomalies in the northwest Atlantic shelf region (~1.7°C) exceeds those found anywhere in the Atlantic and Pacific between 20°S and 60°N, including the active upwelling region off the coast of Peru [*Weare et al.*, 1976; *Weare*, 1977; *Cayan*, 1986].

Early studies of the relationship between North Atlantic SST and the overlying atmosphere were generally qualitative or statistical. In an important and insightful study, *Bjerknes* [1964] hypothesized that interannual changes in large-scale SST patterns are driven by the atmospheric circulation while the interdecadal changes are related to ocean circulation. This point of view is generally held to this day [e.g., *Gordon et al.*, 1992]. More recently, *Bunker* [1976, 1979] estimated air-sea heat fluxes from ship-of-opportunity observations and confirmed the importance of latent and sensible heat fluxes in changing the SST on seasonal and longer timescales. Statistical analyses have also been carried out on regional scales. For example, *Ratcliffe and Murray* [1970] found an empirical relationship between SST off the coast of Newfoundland and air pressure over Europe 1 month later. In another regional study, *Thompson et al.* [1988] analyzed SST from the shelf-slope region of the northwest Atlantic and proposed that the large-scale winter SST patterns spanning the Scotian Shelf, Gulf of Maine, and Mid Atlantic Bight were related to changes in the onshore-offshore component of the wind which, in turn, modulated the latent and sensible heat fluxes.

More recently, the statistical analyses have been complemented by modeling studies. *Palmer and Sun* [1985] examined the statistical relationship of *Ratcliffe and Murray* [1970] using a general circulation model. They found that a significant atmospheric response over Europe could indeed be associated with SST anomalies in the northwest Atlantic. In a large-scale study featuring a constant mixed layer model, *Cayan* [1992b] showed that the latent and sensible heat fluxes were related to the rate of change of the SST anomalies in the northwest Atlantic.

As part of an ongoing study of SST variability in the northwest Atlantic, we have developed a simple model for upper ocean temperatures based on a modified diffusion equation. Our long-term goal is to determine the origin of the low-frequency SST changes observed in the northwest Atlantic and, in particular, the dramatic decrease from the early 1950s to the mid 1960s. Is the decrease simply due to low-frequency variations in latent and sensible heat fluxes,

Paper number 94JC01620.
0148-0227/94/94JC-01620$05.00

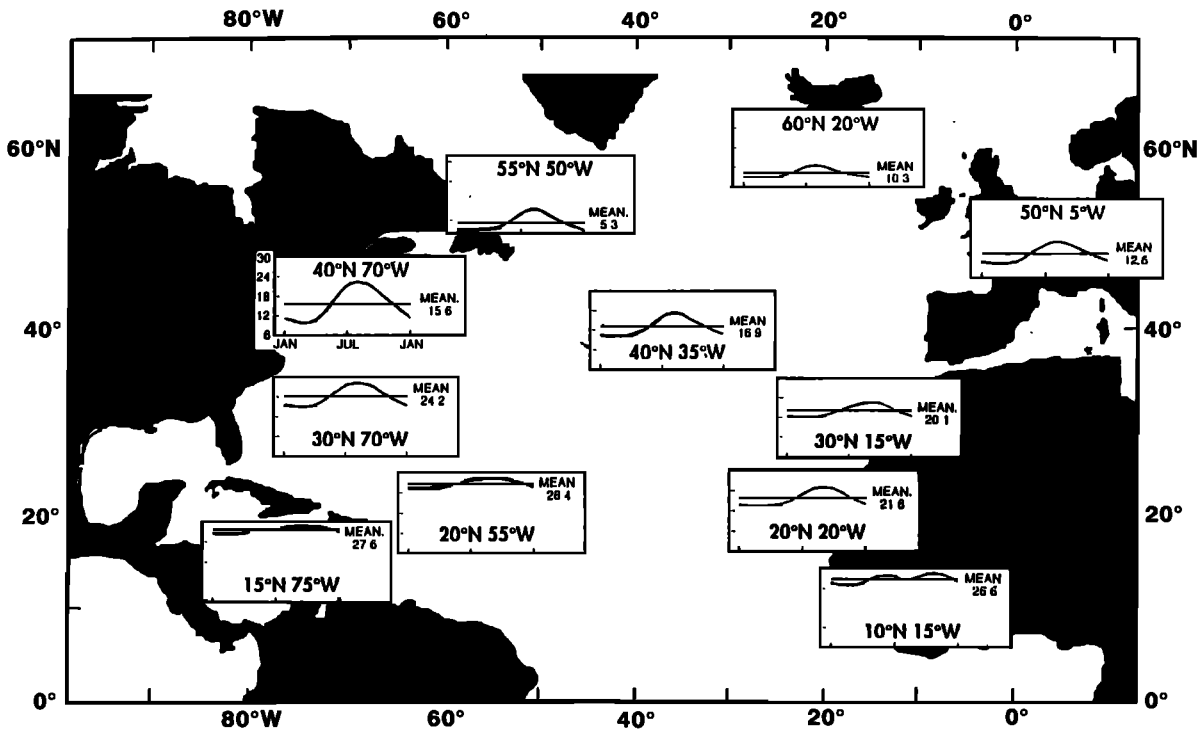

Figure 1. Seasonal cycle of sea surface temperature, in degrees Celsius, for different regions of North Atlantic. All to same scale. Redrawn from *Cayan* [1986].

as proposed by *Thompson et al.* [1988] based on statistical analysis, or is the ocean playing a role, perhaps through horizontal advection? In this paper we focus on the seasonal cycle of water temperature, including its vertical structure, on the Scotian Shelf. Our immediate goal is to explain the pronounced seasonal oscillation in this region using the diffusion model. We also examine the cold intermediate layer, a prominent feature of the Scotian Shelf temperature field, and explain how it is formed.

The novel feature of our analysis is in the diffusion model which has been designed to explain, and be driven by, monthly-averaged data. It therefore has a time step of 1 month. Day-to-day variations in temperature structure, associated with the passage of storms, for example, are not modeled explicitly, but their net effect on the vertical flux of heat over a month is parameterized using a vertical eddy diffusivity, K_v. We show that such a model can do a remarkably good job of simulating the observed temperature changes if we allow K_v to vary with the background density stratification. We also describe a straightforward way of estimating K_v from temperature and salinity data. In a subsequent paper we will use our seasonally calibrated model to examine the low-frequency SST changes in the northwest Atlantic.

This paper is organized as follows. The temperature and salinity data are described in section 2, and the mean and seasonal heat budgets are presented in section 3. The modified heat diffusion model and a method for estimating K_v are given in section 4. The model is used in section 5 to examine the formation of the cold intermediate layer, and the conclusions are presented in section 6.

2. Observations: Sources and Basic Description

The basic data are monthly temperatures and salinities, averaged over many years, at standard depths for 34 subareas of the Scotian Shelf and the Halifax Section (Figure 2a). These data were compiled by *Drinkwater and Taylor* [1982] and *Drinkwater and Trites* [1987]. Definition of the 34 subareas was based on bottom topography (many of the subareas correspond to banks or deep basins) and the availability of sufficient data to form a long-term monthly mean. The individual observations making up the monthly means were made between 1910 and 1982, with about 85% after 1950. In the early years, temperatures were measured using reversing thermometers and salinity by titration; conductivity, temperature, and depth (CTD) probes were generally used after about 1967. Representative time-depth plots of water temperature and salinity are shown in Figure 3.

Monthly heat fluxes, averaged over the period 1941–1972, were obtained from *Isemer and Hasse* [1987] on a 1° × 1° grid covering the North Atlantic. The gridded values were interpolated from means of *Bunker*'s [1976] irregularly shaped areas which, at times, were as large as 10° by 10°. The net heat flux, assumed positive into the ocean, is defined by

$$Q = Q_S - Q_I - Q_L - Q_H \tag{1}$$

where Q_S, Q_I, Q_L, and Q_H are the incoming shortwave radiative flux, the long-wave radiative flux, the latent heat flux, and sensible heat flux respectively. *Isemer and Hasse* [1987] revised the exchange coefficients used by Bunker because recent measurements [*Smith and Dobson*, 1984] show that Bunker's coefficients underestimate Q_S and overestimate Q_L and Q_H.

Other subsidiary data sets include (1) velocities and temperatures from the Scotian Shelf collected as part of the Canadian Atlantic Storms Program (CASP) from November 1985 to March 1986 [*Smith and Anderson*, 1989]; (2) monthly mean wind statistics (such as mean wind speed) from the Comprehensive Ocean-Atmosphere Data Set (COADS),

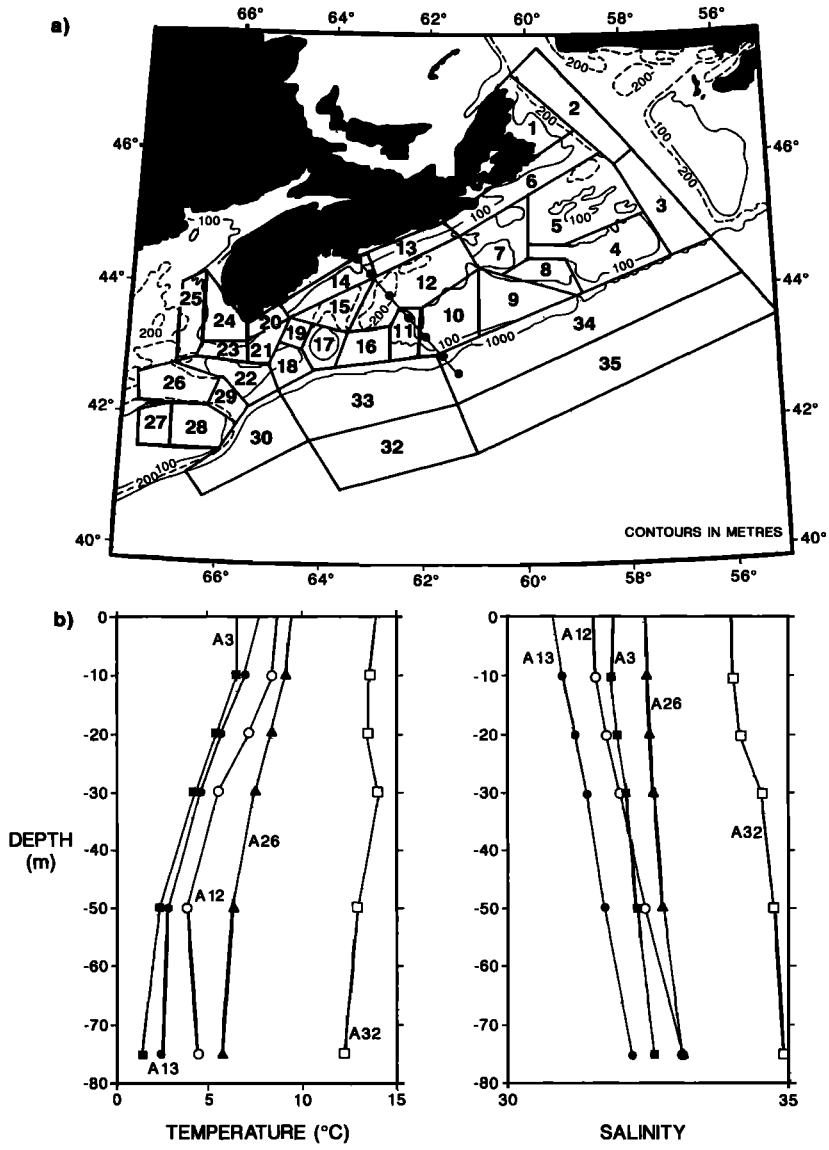

Figure 2. (a) Map of Scotian Shelf showing main topographic features, Halifax Section and the 34 subareas where the long-term mean temperature and salinity were estimated. Emerald Basin is located in subarea A12. The solid circles show the seven stations along the Halifax Section [*Drinkwater and Taylor*, 1982; *Drinkwater and Trites*, 1987]. (b) Long-term annual mean temperature and salinity at standard depths for some selected subareas. Notice the cold intermediate layer for subarea A12.

based on ship measurements over the Scotian Shelf and Slope from 1946–1988.

To reduce the size of the temperature and salinity data set, the monthly mean temperatures and salinities for each subarea and depth have been expressed as the sum of an annual mean, annual cycle, its first harmonic, and an error term. For temperature we have

$$T(z, t) = A_0(z) + A_1(z) \cos \{\omega[t - t_1(z)]\} + A_2(z) \cos \{2\omega[t - t_2(z)]\} + \text{error}, \quad (2)$$

and a similar equation for $S(z, t)$ where A_i and t_i are the amplitude and phase lag (in days) of the annual cycle ($i = 1$) and its first harmonic ($i = 2$). The A_i and t_i have been estimated by minimizing the sum of squared errors.

2.1. Annual Mean Temperature and Salinity

The mean temperature for the Halifax Section (Figure 4) illustrates its cross-shelf structure on the Scotian Shelf. The mean temperature generally decreases shoreward and with depth; the warmest temperatures (>10°C) are found in the surface slope water and the coldest temperatures (<3°C) are at about 50 m, close to shore. Across the outer shelf the isotherms are relatively flat. Note the cold intermediate layer centered at about 50 m on the midshelf. The mean salinities are lowest close to the surface and the coast (<31), and increase to over 34 in the deeper slope water (Figure 4). Note that unlike the mean temperature, the mean salinity increases monotonically with depth.

Using the mean density field, we infer a southwestward geostrophic current along the coast (the Nova Scotia Current

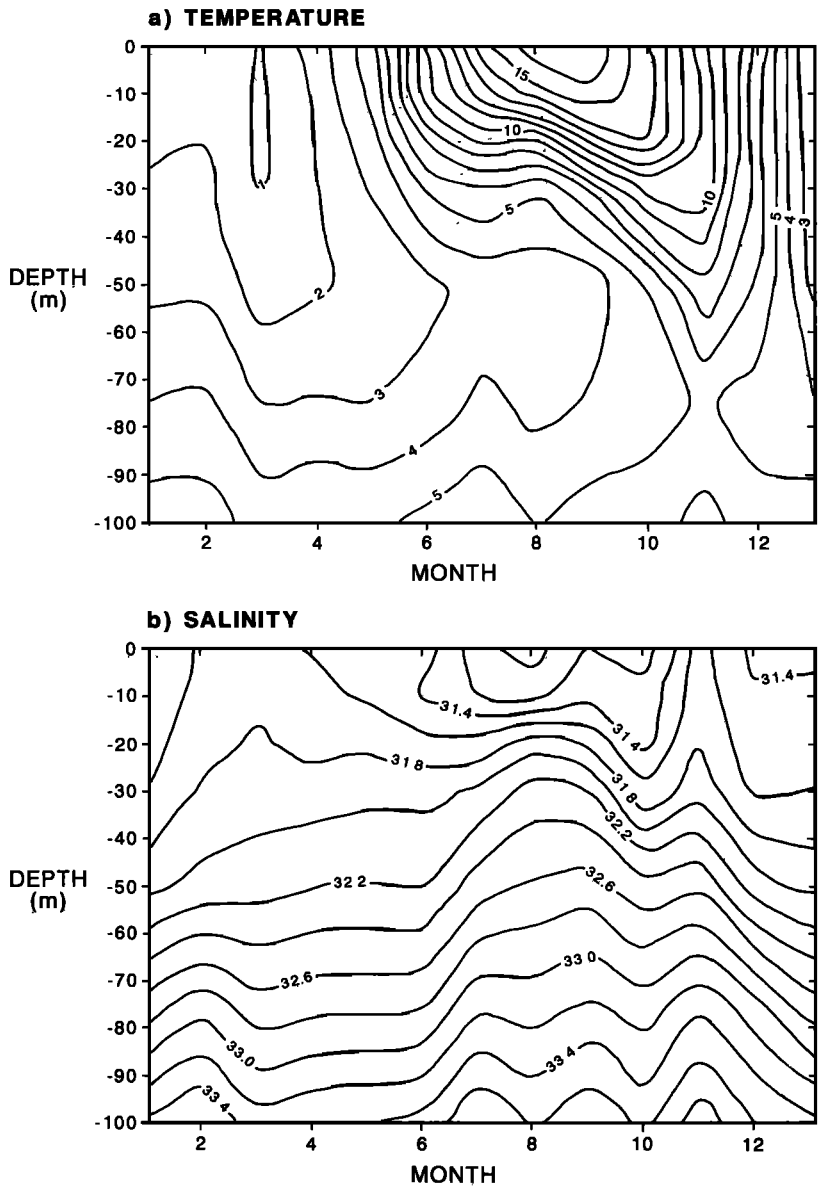

Figure 3. Observed (a) temperature in degrees Celsius (contour interval is 1°C) and (b) salinity for Emerald Basin.

[*Drinkwater et al.*, 1979]) and shelf break [*Csanady*, 1979] of about 4×10^{-2} m s^{-1} relative to 75 m. The implied baroclinic shear is consistent with observations [*Drinkwater et al.*, 1979; *Smith*, 1983; *Smith and Schwing*, 1991].

2.2. Annual Cycle of Temperature and Salinity

Along the Halifax Section the amplitude of the annual cycle in temperature increases from about 8°C at the surface to less than 1°C at 75 m (Figure 5a). Below this depth the standard error of the amplitude is so large that the null hypothesis of a constant temperature cannot be rejected at the 5% significance level. Overall, the isopleths of amplitude and phase are fairly level. There is, however, clear evidence in this figure that the amplitude attenuates, and the phase lag increases, with depth. This is suggestive of a temperature signal forced at the surface and diffusing down into the deeper layers of the ocean. The corresponding picture for salinity (Figure 5b) is of an annual cycle that is strongest in the surface coastal waters and the deep slope water. Over the shelf the highest salinities are usually attained in early March near the surface and in October–November at 70 m.

Alongshore advection can be estimated from the variation in the phase of the annual salinity cycle along the shelf. At the surface the phase lag between Misain Bank (A5) and Roseway Basin (A21) (Figure 2a) is about 90 days. Given that they are separated by about 500 km, we obtain a mean westward surface drift of about 6.4×10^{-2} m s^{-1}, comparable with estimates from drifters [*Drinkwater et al.*, 1979]. The inferred speed of the westward drift decreases with depth. At 30 m the corresponding phase lag is about 197 days, corresponding to a speed of about 2.9×10^{-2} m s^{-1}.

The semiannual amplitude for temperature is typically one-tenth that of the annual cycle. It has a secondary maximum between 30 m and 50 m depth, similar to that observed on the

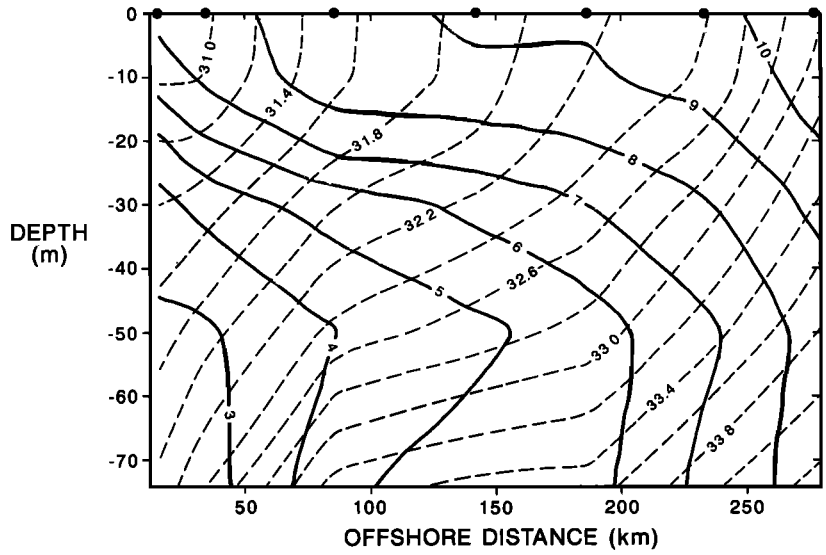

Figure 4. Long-term mean temperature in degrees Celsius (solid line) and salinity (dotted line) for Halifax Section. The solid circles show the seven stations along the section.

eastern Newfoundland shelf [*Petrie et al.*, 1991]. The semiannual amplitude for salinity is also small: about 0.1 at the surface. We will not discuss further the semiannual cycle in temperature or salinity.

3. Heat Budget

Based on the above description, it appears that surface forcing and horizontal advection are potentially important contributors to the seasonal evolution of temperature on the Scotian Shelf. We now attempt to quantify the contribution of these processes, along with that of mixing and upwelling. In this section we focus on Emerald Basin, which is representative of other areas on the mid-Scotian Shelf and also an area with a relatively large number of observations. Heat and salt budgets for coastal and slope regions are presented by *Umoh* [1992].

The equation governing the rate of change of heat stored between the surface ($z = 0$) and some bottom reference level ($z = -h$) is assumed to be [e.g., *Bryan and Schroeder*, 1960; *Merle*, 1980; *Frankignoul and Reynolds*, 1983]

$$\frac{\partial H}{\partial t} = Q - \rho c_p \int_{-h}^{0} \left(\mathbf{u} \cdot \nabla T + w \frac{\partial T}{\partial z} - K_H \nabla^2 T \right) dz - \rho c_p K_v \left. \frac{\partial T}{\partial z} \right|_{-h} \quad (3)$$

where $H = \rho c_p \int_{-h}^{0} T\, dz$, $\mathbf{u} = (u, v)$ is the horizontal water velocity with u cross-shore and v alongshore, w is the vertical velocity and $\nabla = (\partial/\partial x, \partial/\partial y)$. The rest of the notation is standard.

3.1. Local Heat Storage and Surface Flux

The rate of change of heat storage, the left-hand side of (3), is shown in Figure 6a for Emerald Basin. We took h = 75 m which, as discussed earlier, is the average penetration depth of the annual temperature signal. The maximum rate of heat gain (200 W m^{-2}) is in June and maximum heat loss (−400 W m^{-2}) is in December.

Monthly estimates of Q for Emerald Basin, obtained by spatial interpolation of *Isemer and Hasse*'s [1987] gridded values, are shown in Figure 6a. About 85% of the variance in $\partial H/\partial t$ is explained by Q. The amplitude of the annual cycle of the difference between Q and $\partial H/\partial t$ (obtained by fitting an annual cycle to the difference) is 30 W m^{-2}. To fit this discrepancy into a regional perspective, the amplitude of $\partial H/\partial t - Q$ was calculated for each of the remaining 33 subareas. In each subarea, Q and $\partial H/\partial t$ were computed separately and the annual amplitude of the difference $\partial H/\partial t - Q$ estimated. The annual amplitude of the difference contoured across the whole Scotian Shelf is shown in Figure 7. Note that the discrepancy is relatively small (<40 W m^{-2}) over the western end of the mid-Scotian Shelf, indicating a local response of the temperature field to surface forcing by Q. The large difference in Q and $\partial H/\partial t$ for the eastern end of the shelf is probably due to the advection of colder water from the Gulf of St. Lawrence.

3.2. Horizontal Advection

The horizontal velocity was assumed to be of the form

$$\mathbf{u} = \mathbf{u}_E + \mathbf{u}_G \quad (4)$$

where $\mathbf{u}_E$ and $\mathbf{u}_G$ denote long-term monthly mean Ekman and geostrophic velocities, respectively. The wind stress (τ), used to calculate the Ekman velocities, was estimated from

$$\tau = \rho_a c_d (\overline{|\mathbf{u}_a|}) \overline{|\mathbf{u}_a| \mathbf{u}_a} \quad (5)$$

where $\mathbf{u}_a$ is the wind velocity, ρ_a = 1.2 kg m^{-3} is the air density, and an overbar denotes a monthly mean. The monthly wind statistics (mean speed, $\overline{|\mathbf{u}_a|}$, and "pseudo-stress", $\overline{|\mathbf{u}_a| \mathbf{u}_a}$) were obtained directly from COADS. The drag coefficient c_d was assumed to vary with wind speed according to the formula of *Large and Pond* [1981]. The Ekman transport was distributed uniformly over the top 15 m. The absolute geostrophic velocities, $\mathbf{u}_G$, were calculated

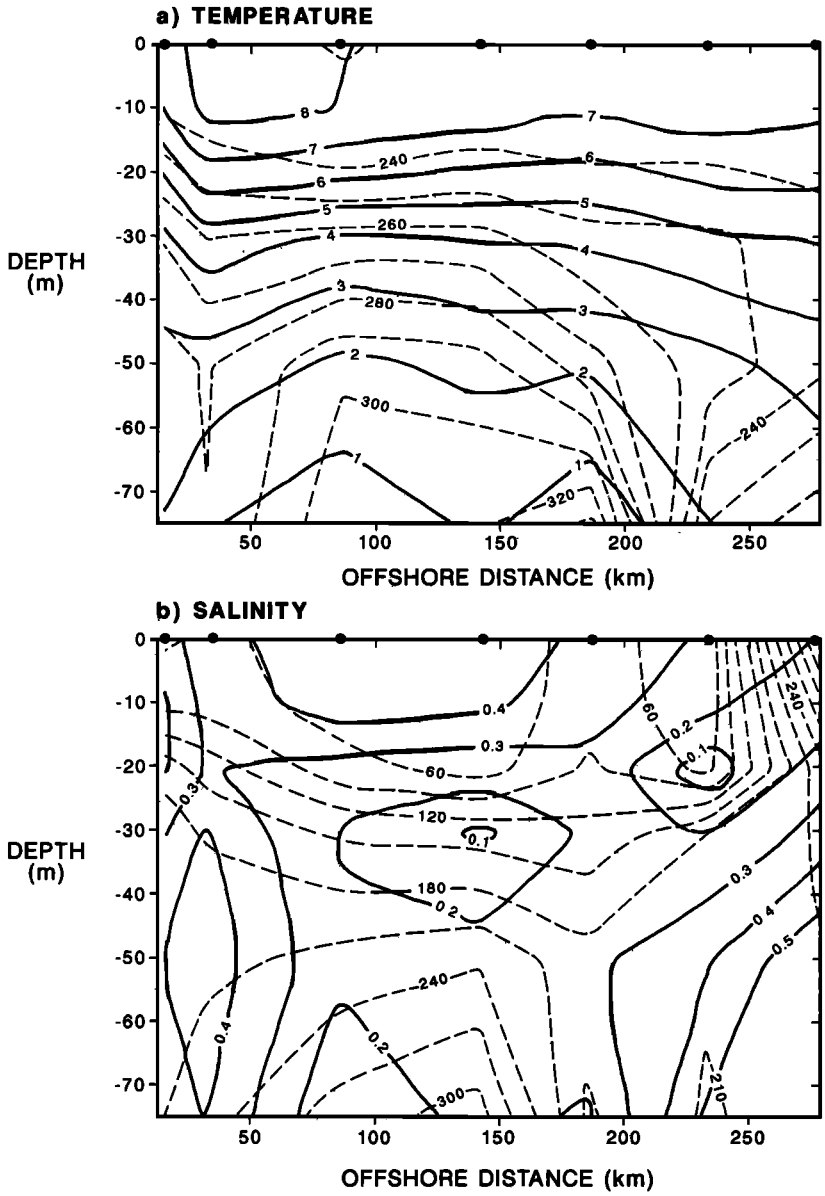

Figure 5. Amplitude and phase of the annual cycle in hydrography for Halifax Section. The amplitude (solid line) and the phase (dotted line, day of the year that the annual cycle achieves its maximum) for (a) temperature in degrees Celsius and (b) salinity.

from density data for Emerald Basin and the surrounding subareas, using the thermal wind relationship and a level of no motion at 100 m. This choice of level of no motion was based, in part, on results presented by *Smith and Schwing* [1991]. They showed that although the flow at 100 m was not negligible over the inner portion of the shelf, it decreased considerably with distance from shore. In the absence of direct current measurement at depth in Emerald Basin, we simply assumed a level of no motion at 100 m. If, in fact, there is a flow at depth of about 5×10^{-2} m s^{-1}, comparable to that observed at the deepest of the moorings examined by *Smith and Schwing* [1991], this would lead to an error in our estimates of the advective current of about 20%.

Monthly heat fluxes due to horizontal advection are generally negative with an annual mean of -40 W m^{-2} (Figure 6b). This is presumably the cooling effect of colder water coming onto the Scotian Shelf from the Gulf of St. Lawrence and further north. There is some evidence of seasonality in this advective flux, with the strongest contributions in late winter and early spring.

3.3. Ekman Upwelling

Vertical velocities were calculated using the standard formula for open ocean upwelling ($w_E = \mathbf{k} \cdot \nabla \times (\tau/\rho f)$). Clearly this formula will not apply to areas within a few internal Rossby radii (about 15 km) of the coast but should be acceptable for Emerald Basin. Our w_E compare well with previous estimates [*Thompson and Hazen*, 1983; *Isemer and Hasse*, 1987] and range from 0.3×10^{-6} m s^{-1} in September to 1.3×10^{-6} m s^{-1} in May. To compute the heat flux, we assume w_E is uniform between 75 m and 15 m depth and then decreases linearly to zero at the sea surface. We also used the observed temperatures to estimate the vertical temperature gradient at various depths. The monthly upwelling heat

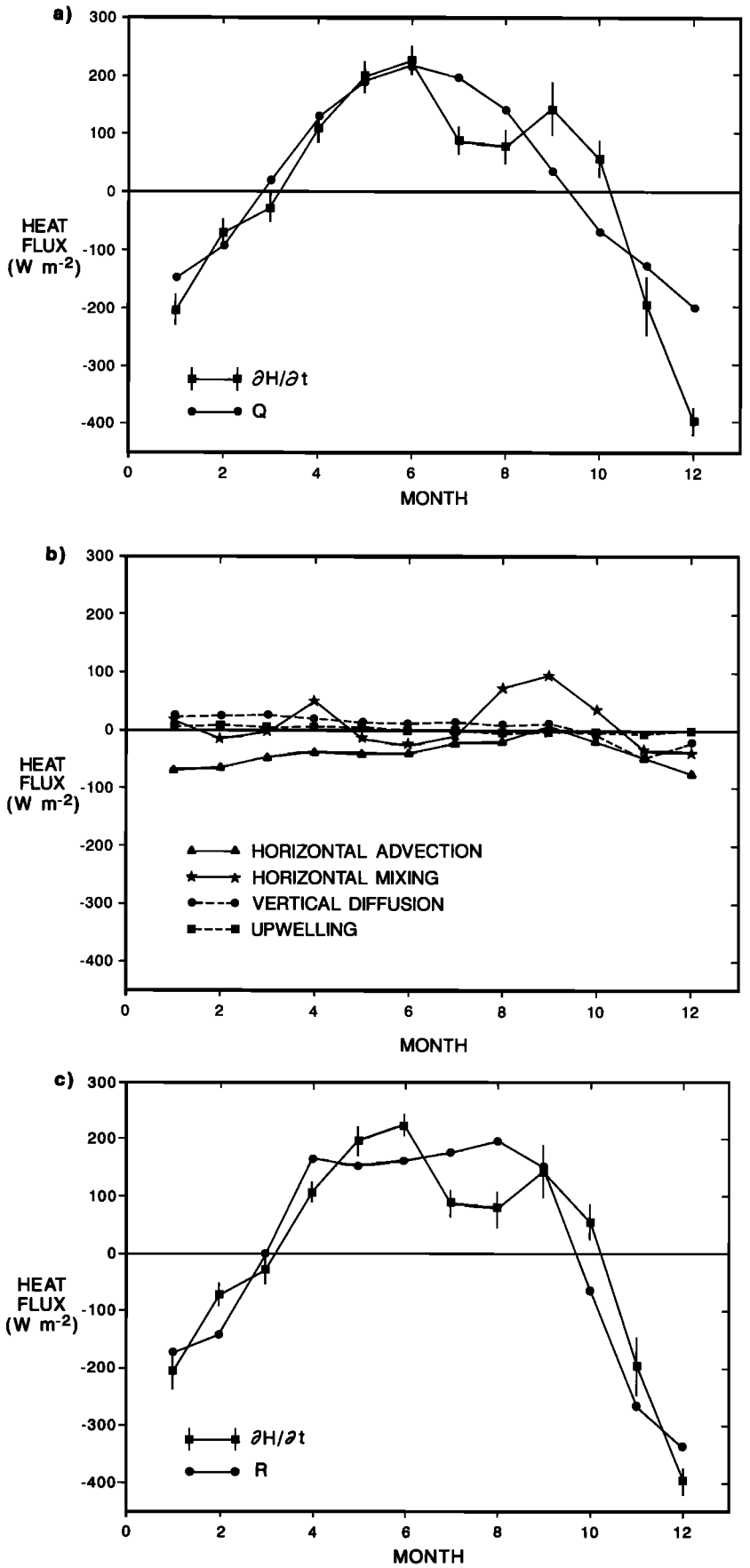

Figure 6. Monthly estimates of the terms in the seasonal heat budget for Emerald Basin. (a) Q and $\partial H/\partial t$. The vertical lines define a 95% confidence interval for $\partial H/\partial t$. (b) Horizontal advection HA, upwelling UP, horizontal mixing HM, and vertical diffusion VD at 75 m. (c) R and $\partial H/\partial t$ ($R = Q +$ HA + UP + HM + VD).

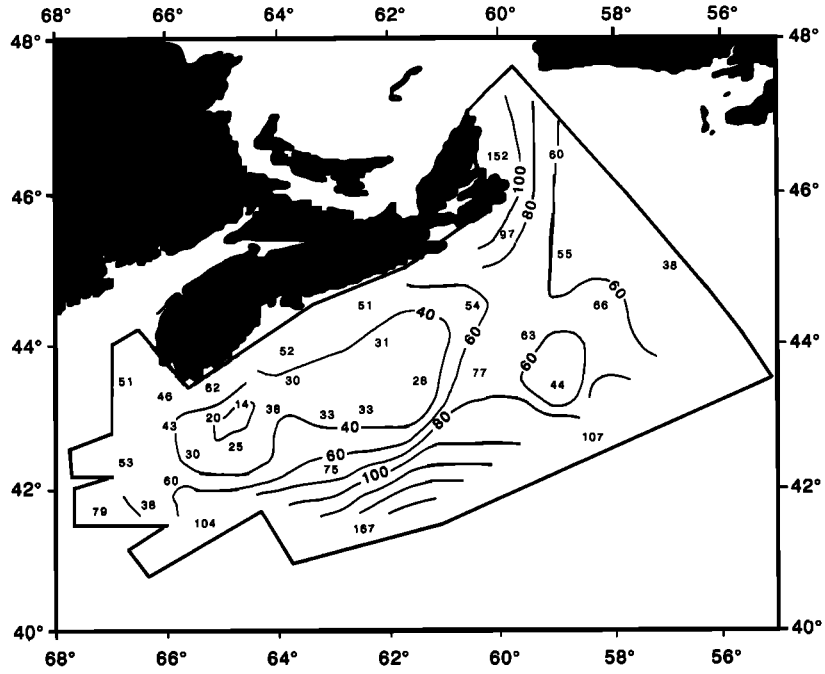

Figure 7. Map of the annual amplitude of the difference $\partial H/\partial t - Q$ in watts per square meter. The contour interval is 20 W m^{-2}. The small numerals are the values for each subarea. Q was obtained by spatial interpolation of *Isemer and Hasse*'s [1987] gridded values to the center of each subarea.

fluxes are generally small. They are all less than 10 W m^{-2} in absolute value and have an annual mean of only 1 W m^{-2} (Figure 6b).

3.4. Horizontal Mixing

The most difficult part of this calculation is the choice of a value for K_H. We used temperature and velocity data from CASP to estimate K_H from the equations

$$K_x \partial \bar{T}/\partial x = -\overline{u'T'} \qquad K_y \partial \bar{T}/\partial y = -\overline{v'T'} \qquad (6)$$

where an overbar denotes a monthly mean and a prime a deviation from the monthly mean. K_x and K_y were determined from the covariance between $\partial \bar{T}/\partial x$ and $-\overline{u'T'}$, and $\partial \bar{T}/\partial y$ and $-\overline{v'T'}$ using principal component analysis (see *Umoh* [1992] for details). We found K_x = 679 m^2 s^{-1}, K_y = 546 m^2 s^{-1}, although both are subject to large uncertainty. Note, however, that they are in line with previous estimates of horizontal diffusivity for the shelf [e.g., *Garrett et al.*, 1985]. Although the annual mean contribution from horizontal mixing is small, it is not negligible at certain times of the year (~100 W m^{-2} in late summer (Figure 6)).

3.5. Vertical Diffusion

A constant diffusivity of 10^{-4} m^2 s^{-1} at $z = -h$ was used. We will show later that this is a reasonable assumption. Overall, there is a diffusive heat flux from the deep ocean into the surface layers with an annual mean of about 10 W m^{-2} (Figure 6b).

3.6. Does the Heat Budget Balance?

The dominant term in the long-term annual mean budget for Emerald Basin is cooling due to horizontal advection (Table 1). The mean budget is balanced to within about 10% of the largest term by the combined effects of Q, horizontal mixing, and vertical diffusion. Given the errors in the data, as discussed below, such a small imbalance is almost certainly fortuitous.

The seasonal heat budget for Emerald Basin is more straightforward: to first order, the rate of change of heat content is simply due to Q (Table 2). If we combine horizontal advection and Q, together they account for 99% of the amplitude of $\partial H/\partial t$. Inclusion of the other terms does not improve the seasonal heat budget.

The imbalances in both mean and seasonal heat budgets are due in part to observation errors. For Emerald Basin, errors in the long-term monthly mean temperatures (estimated by $s/n^{1/2}$, where s and n are the sample standard deviation and the number of observations contributing to each mean) cause standard errors in $\partial H/\partial t$ of 18–50 W m^{-2} as shown in Figure 6a. Another source of error in the monthly temperature data is that the individual observations were not necessarily spaced regularly over the month and so a bias can arise from the large (~5°C) seasonal temperature change that can occur over the course of a month, particularly in spring and fall. No attempt was made to correct for this error.

It is difficult to obtain reliable error estimates for Q, although they are probably of the order of tens of watts per

Table 1. Annual Mean Heat Budget for Emerald Basin

Term	Mean, W m^{-2}
Horizontal advection	−40
Surface heat flux	25
Horizontal mixing	11
Vertical diffusion	6
Upwelling	1
Imbalance	3

Table 2. Seasonal Heat Budget for Emerald Basin

Term	Amplitude, W m^{-2}	Phase, day
Local rate of heat storage	222	159
Surface heat flux (Q)	202	153
Horizontal advection (HA)	26	203
Horizontal mixing (HM)	25	217
Vertical diffusion (VD)	20	95
Upwelling (UP)	6	64
Vector sum of Q + HA	220	158
Imbalance	2	1
Vector sum of Q + HA + HM + VD + UP	244	158
Imbalance	22	1

The amplitude was obtained by fitting an annual cycle to the data and phase was relative to January 1.

square meter [e.g., *Isemer et al.*, 1989; *Cayan*, 1992a]. The interpolation of *Bunker*'s [1976] original data onto the 1° grid introduces another type of error that is difficult to quantify. The fact that $\partial H/\partial t$ and Q agree so well is, in some respects, an encouraging result given that they were estimated from essentially independent data sets.

Our estimate of K_H has large error bars [*Umoh*, 1992], although we note that it is in line with previous work. Fortunately, horizontal mixing is not a major contributor to the heat budget on a seasonal timescale, except in July and August. The discrepancy between $\partial H/\partial t$ and other terms in July and August (Figures 6a and 6c) may be caused by horizontal mixing (Figure 6b), bringing warm Gulf Stream water onto the shelf. Unfortunately, horizontal mixing is generally not negligible on longer timescales and will pose a serious challenge to modelers of interannual variability in this region.

4. Modeling the Vertical Temperature Structure

We have seen that most of the seasonal variation of $\partial H/\partial t$ on the mid-Scotian Shelf can be explained by Q and horizontal advection. We now attempt to explain the seasonal variation in the vertical temperature structure. Our approach is to use a one-dimensional diffusion model, modified to include the effect of advection. The reason we have employed such a model, instead of a more conventional upper ocean model such as that of *Kraus and Turner* [1967] or *Price et al.* [1986], is that the data available to drive our model (e.g., Q) are monthly means and so we cannot simulate explicitly the episodic deepening and shallowing of the mixed layer associated with the passage of storms, and their effects on the monthly mean temperature profile. In our model such high-frequency variations are averaged out, and their mean effect is parameterized using an effective vertical diffusivity.

4.1. Modified Diffusion Model

We assume the seasonal evolution of temperature on the mid-Scotian Shelf satisfies

$$\frac{\partial T}{\partial t} = \frac{\partial}{\partial z}\left(K_v \frac{\partial T}{\partial z}\right) + \Gamma \tag{7}$$

where $\Gamma(z, t)$ is a source-sink term which from (3) includes horizontal advection, upwelling, horizontal mixing, and vertical diffusion, but as shown in the previous section, is due primarily to horizontal advection. To use this equation we need not only the boundary conditions, which we can obtain from observations, but also Γ and K_v.

$\Gamma(z, t)$ can be estimated in different ways. We initially estimated it directly from observations. However, the estimates were very noisy. We therefore adopted the following approach. First, we depth-integrated (7) from $z = -h$ to $z = 0$ and obtained

$$\rho c_p h\langle\Gamma\rangle = \frac{\partial H}{\partial t} - Q + \rho c_p K_v \frac{\partial T}{\partial z}\bigg|_{-h}, \tag{8}$$

where angle brackets correspond to the depth-averaging operator $h^{-1}\int_{-h}^{0} dz$. Note that all the terms on the right-hand side of (8) can be estimated from observations, as discussed in the previous section. (We used $K_v = 10^{-4}$ m^2 s^{-1} at $z = -h$, which we will show to be a reasonable assumption.) Thus the depth mean of Γ is known. Next, we made the important assumption that Γ is a separable function of z and t:

$$\Gamma(z, t) = \alpha(t)\zeta(z). \tag{9}$$

Assuming, without loss of generality, that $\langle\zeta\rangle = 1$ it follows that

$$\alpha(t) = \langle\Gamma\rangle \tag{10}$$

and hence can be considered known. Based on the seasonal heat budget for Emerald Basin, we expect Γ to be due mostly to advection. Given that the strongest alongshore currents and temperature gradients (Figure 3a) are near surface, we further assume that ζ takes the following form:

$$\zeta = e^{z/\delta}/\delta(1 - e^{-h/\delta}). \tag{11}$$

Thus we have reduced the problem of specifying Γ to specifying δ, the e-folding scale for the advective component.

It remains to specify K_v. We assume K_v is related to the vertical density profile according to

$$K_v = K_0(1 + \alpha N^p)^{-1} \tag{12}$$

where N^2 is the Brunt-Väisälä frequency. This is a modification of earlier diffusivity parameterizations [e.g., *Munk and Anderson*, 1948; *James*, 1977; *Henderson-Sellers*, 1982] in which K_v depends explicitly on the Richardson number. Although such parameterizations have produced good results [*Henderson-Sellers*, 1982], they could not be used in this study because velocity shears (upon which the Richardson number depends) were not available. The main advantage of the simpler parameterization given by (12) is that it does not depend directly on the current shear; that information is absorbed in α which we take to be constant.

The procedure for estimating the three unknown diffusivity parameters (K_0, α, and p) and the e-folding advective scale (δ) is both statistical and straightforward. We first express (7) in finite-difference form using a Crank-Nicholson scheme which is second-order accurate in both space and time and stable for arbitrarily large time steps [e.g., *Press et al.*, 1986]. A regular computational grid was used with a time step of 1 month and a uniform vertical spacing of 10 m between $z = -100$ m and $z = 0$ m. The next step is to

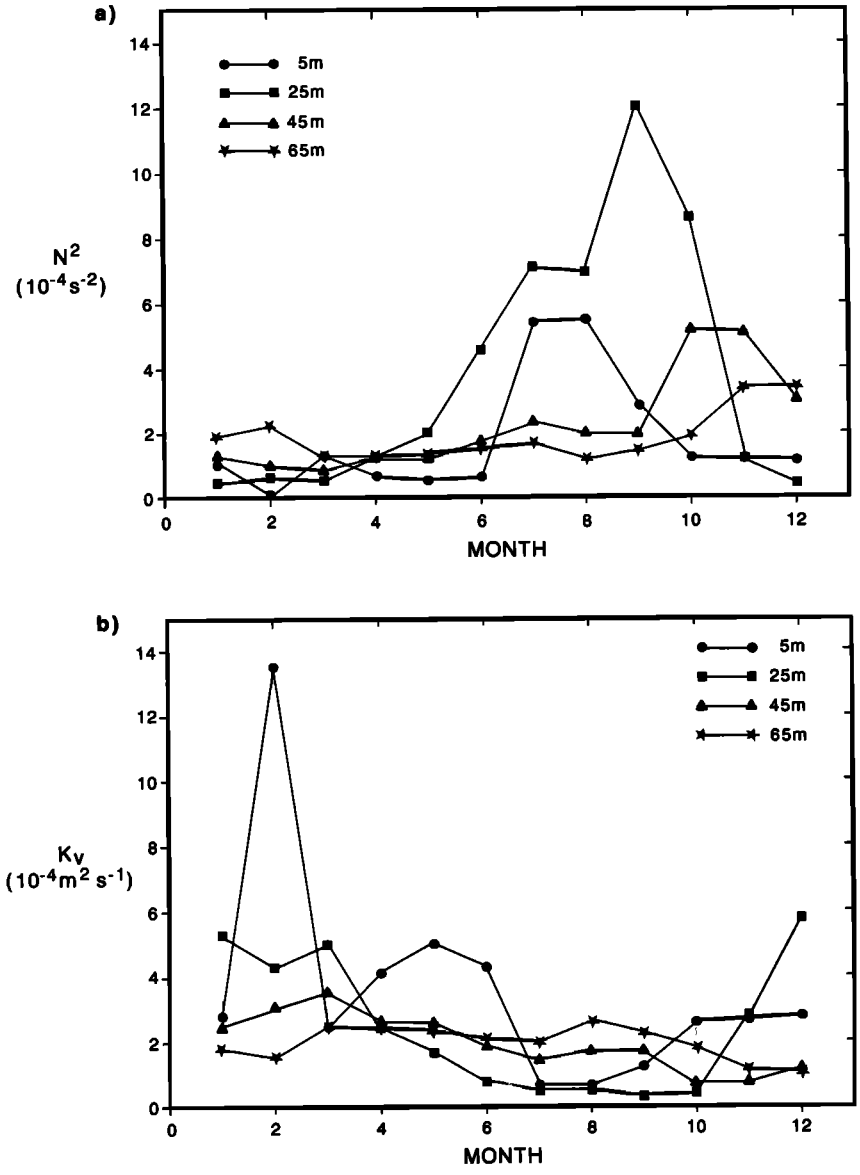

Figure 8. Monthly estimates of (a) N^2 and (b) K_v at different depths for Emerald Basin.

specify the four unknown parameters and use observations for Emerald Basin with (9) and (12) to calculate Γ and K_v at every grid point in the model. It is then possible to integrate the model forward in time, forcing it with Q at the surface and the observed temperature (T_b) at $z = -h$, until the predicted temperatures reach a periodic steady state. We then calculate the root mean square error between observed (T) and predicted ($\hat{T}$) temperatures using

$$E(\delta, p, K_0, \alpha) = \left(\frac{1}{N}\sum_t \sum_z (T - \hat{T})^2\right)^{1/2} \quad (13)$$

where $N = 10 \times 12$ is the total number of grid points in the vertical times months in the final year of integration. By systematically adjusting the four parameters it is possible to find the set that minimizes E. Note that this parameter estimation method can easily be modified to find the best fitting constant K_v by simply setting $\alpha = 0$.

4.2. Results

We experimented with δ in the range [0, 100 m] and $p = 1$, 2, and 4 and found the optimal choices to be $p = 2$ and $\delta = 60$ m. From contour plots of E as a function of K_0 and α (not shown) it is clear that these two parameters covary: a low value of K_0 can be compensated for by a low value of α, and a high value of K_0 by a high value of α. It is thus the ratio of these two parameters that is important. We found that the best fitting parameters for Emerald Basin are $K_{0c} = 15 \times 10^{-4}$ m^2 s^{-1} and $\alpha_c = 4.00 \times 10^4$ s^2.

Diffusivities calculated using $K_v = K_{0c}(1 + \alpha_c N^2)^{-1}$ ranged from 0.2 to 20 $\times$ 10^{-4} m^2 s^{-1}. Note the strong seasonality in K_v evident in Figure 8b: K_v is generally high in winter, when the density stratification is weak, and low in summer when stratification is strong (Figure 8a). It is also apparent from the figure that K_v and its seasonal variation decrease with depth.

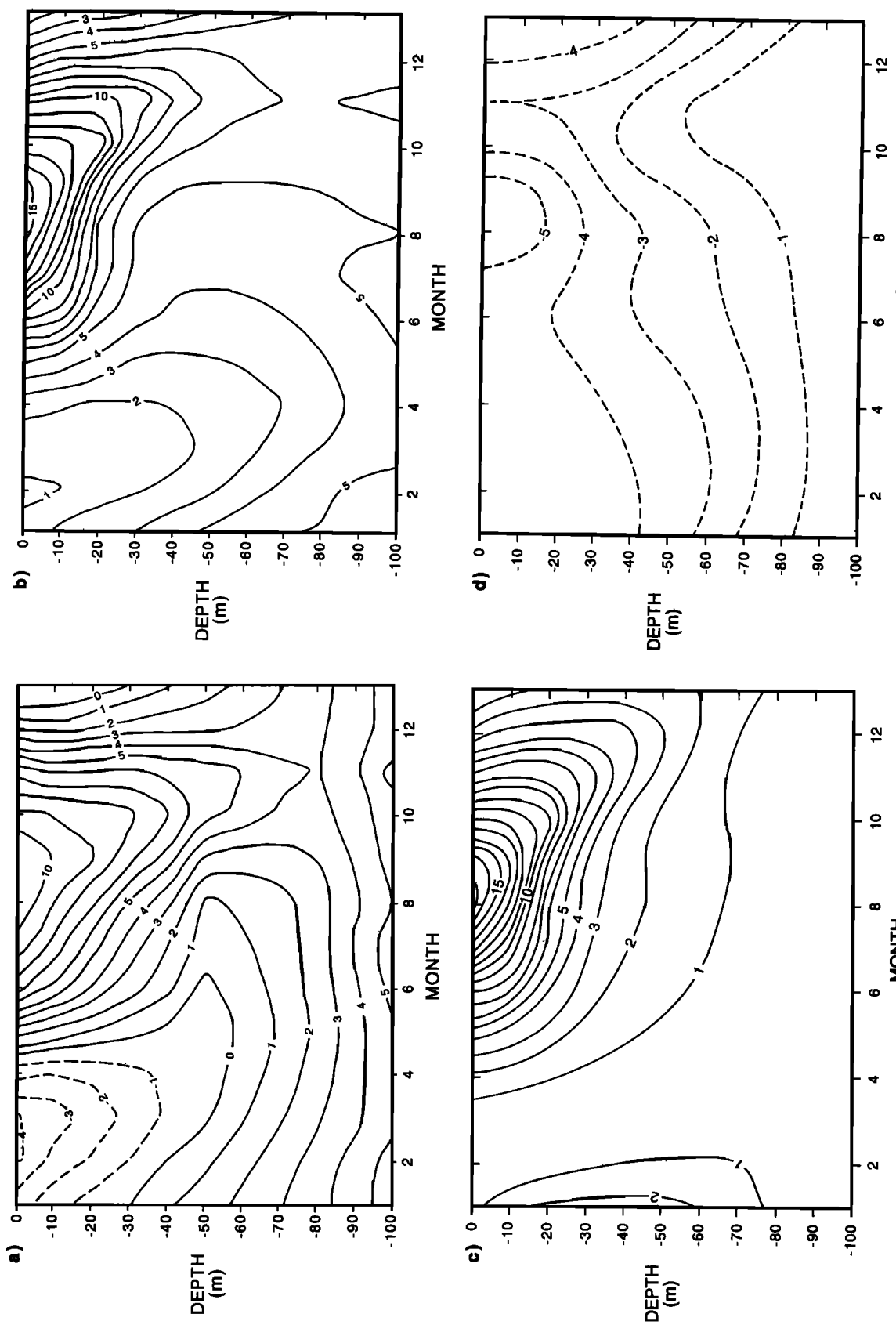

Figure 9. Predicted temperature with constant K_v or seasonal-varying $K_v(z, t)$ forced by various combinations of Q, Γ and observed temperature at $z = -h$, T_b. (a) Constant K_v and forcing by Q, Γ, and T_b, (b) $K_v(z, t)$ and forcing by Q, Γ, and T_b, (c) $K_v(z, t)$ and forcing by Q alone, and (d) $K_v(z, t)$ and forcing by Γ alone.

The predicted temperatures (Figure 9b) using the above K_v values compare well with observations (Figure 3a). We emphasize that the good fit is not the result of overfitting to the $N = 120$ monthly mean temperatures: it has been achieved with only four free parameters. The root mean square error is $E = 0.98$°C. If we use a constant K_v model to the Emerald Basin observations, the minimum E increases from 0.98°C to 3.11°C and the optimal constant K_v is 1.2×10^{-4} m^2 s^{-1}. Although this simpler model can reproduce the overall pattern of temperature variability (Figure 9a), it grossly underestimates the surface temperature. It also overestimates (underestimates) the depth of penetration of the surface-forced temperature signal in summer (winter). We conclude that it is necessary to allow K_v to vary with season and depth if the vertical structure is to be modeled accurately.

5. The Cold Intermediate Layer

A distinctive feature of the Scotian Shelf temperature distribution is a cold intermediate layer that forms from April and September at depths of 50 to 100 m (e.g., *Hachey* [1938]; and Figure 3). This subsurface temperature minimum is also evident in the long-term mean temperature profile for the midshelf (see A12 in Figure 2b).

The cold intermediate layer is not limited to the Scotian Shelf; it has been observed on the Labrador and Northeast Newfoundland Shelves [*Petrie et al.*, 1988] and also in the Gulf of Maine [*Brown and Beardsley*, 1978]. The origin of the cold intermediate layer on the Scotian Shelf was initially discussed by *Hachey* [1938]. From the February TS diagrams, Hachey inferred that the water on the Scotian Shelf is a mixture of two water masses: cold water from the Gulf of St. Lawrence/Labrador current and warm slope water (see also *Gatien* [1976]). He also estimated the alongshore volume transport in February and in June. His estimates (which also agree with those of *Drinkwater et al.* [1979]) showed that the alongshore volume transport in February was about twice that in June. He went on to argue that the cold intermediate layer "is therefore the result of the volume transport of water." (p. 41).

In this section we show that both surface forcing and advection are required to maintain the long-term mean cold intermediate layer. To see this, note that the time average of (8) implies

$$h\langle\bar{\Gamma}\rangle = -\frac{\bar{Q}}{\rho c_p} + K_v \left.\frac{\partial \bar{T}}{\partial z}\right|_{-h} \tag{14}$$

where an overbar signifies a long-term mean and we have assumed, for simplicity, that K_v is constant through time. If $\bar{T}$ has a single minimum at some intermediate depth, then $\partial\bar{T}/\partial z > 0$ at $z = 0$ and $\partial\bar{T}/\partial z < 0$ at $z = -h$. Combining these constraints with (14), it is clear that necessary conditions for the maintenance of a permanent cold intermediate layer are

$$\bar{Q} > 0 \qquad \langle\bar{\Gamma}\rangle < -\frac{\bar{Q}}{h\rho c_p}. \tag{15}$$

This simply means that heating of the cold intermediate layer from above and below must be balanced by a subsurface heat sink. If the layer is now allowed to be transient, there are several ways it could form. These include the passage of a cold water parcel at some intermediate depth, a rapid change in the net surface heat flux from cooling to warming of the ocean, and a combination of fall cooling and spring/summer surface warming through vertical and horizontal mixing [*Narayanan et al.*, 1991]. The above conditions were also derived under the simplifying assumption that K_v is constant through time, allowing the covariance of K_v and $\partial T/\partial z$ to be ignored.

We now extend our discussion to include time dependence in Q, Γ, and K_v. In particular, we use our diffusion model, which we have already shown can reproduce the cold intermediate layer (Figure 9b), to examine the individual contribution of surface forcing and horizontal advection. Such an approach is possible because the diffusion model is linear with respect to these two forcing terms and hence the temperature response can be calculated with either Q or Γ set individually to zero. Note, however, that this approach does not allow for the change in Q that may result from the change in sea surface temperature associated with a change in Γ. Likewise the change in $T(-h, t)$ associated with a change in Q or Γ and its effect on the overlying temperature structure are also ignored.

5.1. Contribution of Q

The model has been run into a periodic steady state with surface forcing by the observed Q, and with Γ and $T(-h, t)$ both set to zero. This is an attempt to determine the seasonal evolution of temperature caused by the surface heat flux alone. The deep temperature is held at some fixed reservoir value, and the surface flux remains the same as that calculated by *Isemer and Hasse* [1987]. Note $\bar{Q} > 0$ and so there is a long-term surface heat flux into the ocean. The model achieves a periodic steady state by diffusing heat across the bottom reference level.

The overall predicted temperature distribution for this case ($T_Q(z, t)$, Figure 9c) is qualitatively similar to that observed (Figure 3), in accord with our earlier result that most of the local rate of heat storage is due to Q. There is, however, an important difference: T_Q does not have a cold intermediate layer in summer, as observed. This discrepancy is not surprising given that we have violated one of the conditions in (15). Even though we have relaxed the assumptions of time-independent K_v and T, we conclude that surface forcing alone is not capable of producing a permanent cold intermediate layer in Emerald Basin.

5.2. Contribution of Γ

The model has also been run into a steady state with Q and $T(-h, t)$ set to zero, and with Γ from (8). This is an attempt to determine the contribution of horizontal advection to the seasonal evolution of temperature in Emerald Basin. The predicted temperature distribution ($T_\Gamma(z, t)$, Figure 9d) shows clearly the net cooling effect of Γ, with the surface temperature about 4°C lower than the bottom temperature. The raising of the T_Γ isopleths in September and October can be traced back to an imbalance in the seasonal heat budget, and in particular a sharp increase in $\partial H/\partial t$ which could not be explained by either Q or $K_v\partial T/\partial z$ at $z = -h$ in these months (see Figure 6). It is also clear that Γ alone does not form a cold intermediate layer in Emerald Basin.

6. Conclusions

The strong seasonal variation in water temperature on the Scotian Shelf is due mainly to the surface heat flux. The net surface heat flux accounts for about 85% of the annual cycle in the rate of change of heat content over the top 75 m of the water column. Upwelling has been suggested as an important contributor to SST variability in summer [e.g., *Bjerknes*, 1964; *Lacy*, 1988]. Our analysis suggests that it makes a negligible contribution to the seasonal heat budget for the mid to outer Scotian Shelf. The contributions from horizontal advection and mixing, and vertical diffusion of heat, are about one-tenth that of Q.

The simplicity of the seasonal heat budget encouraged us to develop a simple diffusion model for the vertical temperature structure. The model uses a K_v that varies with the background density stratification and hence water depth and season. *Umoh* [1992] gives three methods of estimating $K_v(z, t)$. We present in this paper one of the methods. This method guarantees no negative diffusivities (inherent in some methods). The present method of estimating $K_v(z, t)$ depends only on four free parameters. It has the advantage that the $K_v(z, t)$ estimates do not explicitly need velocity data, which are often difficult and expensive to get. It further provides a direct measure of, and indeed, the minimum mean square difference between, the observed and predicted temperatures. We have shown that the best fitting $K_v(z, t)$ values realistically reproduce the $T(z, t)$ structure. The estimated $K_v(z, t)$ ranges from 0.2×10^{-4} m^2 s^{-1} to about 20×10^{-4} m^2 s^{-1} for the upper 75 m. By modifying the method, a constant $K_v = 1.2 \times 10^{-4}$ m^2 s^{-1} was also objectively estimated. The constant K_v reproduces the overall seasonal $T(z, t)$ pattern (low in winter and high in summer) but severely underestimates it. This points out the importance of allowing $K_v(z, t)$ to realistically vary in space and time.

We have applied our model to study the formation of the cold intermediate layer. Warming from the surface (Q) and the deep layers, together with a heat sink at intermediate depths, is required to explain the observed long-term mean cold intermediate layer on the Scotian Shelf. Neither Q nor $\Gamma(z, t)$ alone can produce the cold intermediate layer. It is important to note that although Γ is dominated by horizontal advection, other processes such as horizontal mixing can be important at certain times of the year (see Figure 6b). These findings agree with *Hachey* [1938], insofar as horizontal advection is a contributor to the cold intermediate layer on the Scotian Shelf.

The long-term mean heat budget is more complicated than the seasonal heat budget and highlights the difficulty of modeling interannual changes in this region. Horizontal advection makes the strongest mean contribution (~40 W m^{-2}) and is balanced to within 10% by Q(~25 W m^{-2}) and horizontal mixing (~11 W m^{-2}). On a positive note, the small imbalance in the mean heat budget increases our confidence in our estimates of Q. On the negative side, we note that horizontal mixing, and to a lesser extent horizontal advection, will be extremely difficult to model on interannual timescales with the accuracy required to hindcast SST variability. To illustrate, if we assume that an imbalance of 3 W m^{-2} in the mean heat budget, the result of increasing horizontal mixing, say, is compensated for by an increase in local heat storage, then the change in mean temperature of the top 50 m over 10 years will be $\Delta t Q/\rho c_p h = 4.3$°C. This is significant in comparison to the observed interdecadal variability in this region and indicates the accuracy with which processes like horizontal mixing and advection will have to be modeled. Notwithstanding these potential problems we are currently using our seasonally calibrated diffusion model to isolate the contribution of Q to the interannual temperature variability in this region and will report our findings at a later date.

Acknowledgments. We thank K. Drinkwater and B. Petrie for generously providing the hydrographic data for the Scotian Shelf and Emerald Basin, and J. Loder for useful comments during the preparation of the manuscript. The Canadian Commonwealth Scholarship funded a large portion of J.U.U.'s Ph.D. program, during which time this work was done.

References

Bjerknes, J., Atlantic air-sea interaction, *Adv. Geophys.*, *10*, 1–82, 1964.

Brown, W. S., and R. C. Beardsley, Winter circulation in the western Gulf of Maine, 1, Cooling and water mass formation, *J. Phys. Oceanogr.*, *8*, 265–277, 1978.

Bryan, K., and E. Schroeder, Seasonal heat storage in the North Atlantic Ocean, *J. Meteorol.*, *17*, 670–674, 1960.

Bunker, A. F., Computation of surface energy flux and annual air-sea interaction cycles of the North Atlantic Ocean, *Mon. Weather Rev.*, *104*, 1122–1140, 1976.

Bunker, A. F., Trends of variables and energy fluxes over the Atlantic Ocean from 1948 to 1972, *Mon. Weather Rev.*, *108*, 720–732, 1979.

Cayan, D. R., North Atlantic seasonal sea surface temperature anomalies and associated statistics, 1949–85, *Rep. SIO 85-19*, 89 pp., Scripps Inst. of Oceanogr., La Jolla, Calif., 1986.

Cayan, D. R., Variability of latent and sensible heat fluxes estimated using bulk formulae, *Atmos. Ocean*, *30*, 1–42, 1992a.

Cayan, D. R., Latent and sensible heat flux anomalies over the northern oceans: Driving the sea surface temperature, *J. Phys. Oceanogr.*, *22*, 859–881, 1992b.

Csanady, G. T., The pressure field along the western margin of the North Atlantic, *J. Geophys. Res.*, *84*, 4905–4915, 1979.

Drinkwater, K. F., and G. Taylor, Monthly means of the temperature, salinity and density along the Halifax section, *Can. Tech. Rep. Fish. Aquat. Sci.*, *1093*, 67 pp., 1982.

Drinkwater, K. F., and R. W. Trites, Monthly means of temperature and salinity in the Scotian Shelf region, *Can. Tech. Rep. Fish. Aquat. Sci.*, *1539*, 101 pp., 1987.

Drinkwater, K. F., B. Petrie, and W. H. Sutcliffe Jr., Seasonal geostrophic volume transports along the Scotian Shelf, *Estuarine Coastal Shelf Sci.*, *9*, 17–27, 1979.

Frankignoul, C., and R. W. Reynolds, Testing a dynamical model for mid-latitude sea surface temperature anomalies, *J. Phys. Oceanogr.*, *13*, 1131–1145, 1983.

Garrett, C., J. Middleton, M. Hazen, and F. Majaess, Tidal currents and eddy statistics from iceberg trajectories off Labrador, *Science*, *227*, 1333–1335, 1985.

Gatien, M. G., A study in the slope water region south of Halifax, *J. Fish. Res. Board Can.*, *33*, 2213–2217, 1976.

Gordon, A. L., S. E. Zebiak, and K. Bryan, Climate variability and the Atlantic Ocean, *Eos Trans. AGU*, *73*(15), 161, 164–165, 1992.

Hachey, H. B., The origin of the cold water layer of the Scotian Shelf, *Trans. R. Soc. Can., Ser. 3, Sect. III*, 29–42, 1938.

Henderson-Sellers, B., A simple formula for vertical eddy diffusion coefficients under conditions of nonneutral stability, *J. Geophys. Res.*, *87*, 5860–5864, 1982.

Isemer, H., and L. Hasse, *The Bunker Climate Atlas of the North Atlantic Ocean*, vol. 2, *Air-Sea Interaction*, Springer-Verlag, New York, 1987.

Isemer, H., J. Willebrand, and L. Hasse, Fine adjustment of large scale air-sea energy flux parameterizations by direct estimates of ocean heat transport, *J. Clim.*, *2*, 1173–1184, 1989.

James, I. D., A model of the annual cycle of temperature in a frontal

region of the Celtic Sea, *Estuarine Coastal Mar. Sci.*, *5*, 339–353, 1977.

Kraus, E. B., and J. S. Turner, A one-dimensional model of the seasonal thermocline, II, *Tellus*, *19*, 98–106, 1967.

Lacy, B. J., The coupled atmosphere-ocean system: An analysis of North Atlantic air pressure and sea surface temperature, M.Sc. thesis, 101 pp., Dalhousie Univ., Halifax, N. S., Canada, 1988.

Large, W. G., and S. Pond, Open ocean momentum flux measurement in moderate to strong winds, *J. Phys. Oceanogr.*, *11*, 324–336, 1981.

Merle, J., Seasonal variation of heat storage in the tropical Atlantic Ocean, *Oceanol. Acta*, *3*, 455–463, 1980.

Munk, W. H., and E. R. Anderson, Notes on a theory of the thermocline, *J. Mar. Res.*, *7*, 276–295, 1948.

Narayanan, S., E. B. Colbourne, and C. Fitzpatrick, Frontal oscillations on the NE Newfoundland Shelf, *Atmos. Ocean*, *29*, 547–562, 1991.

Palmer, T. N., and Z. Sun, A modelling and observational study of the relationship between sea surface temperature in the northwest Atlantic and the atmospheric general circulation, *Q. J. R. Meteorol. Soc.*, *111*, 947–975, 1985.

Petrie, B., S. Akenhead, J. Lazier, and J. Loder, The cold intermediate layer on the Labrador and northeast Newfoundland Shelves, 1978–86, *Northwest Atl. Fish. Organ. Sci. Counc. Stud.*, *12*, 57–69, 1988.

Petrie, B., J. W. Loder, S. Akenhead, and J. Lazier, Temperature and salinity variability on the eastern Newfoundland: The annual harmonic, *Atmos. Ocean.*, *29*, 14–36, 1991.

Press, W. H., B. P. Flannery, S. A. Teukolsky, and W. T. Vetterling, *Numerical Recipes*, 818 pp., Cambridge University Press, New York, 1986.

Price, J. F., R. A. Weller, and R. Pinkel, Diurnal cycling: Observation and models of the upper ocean response to diurnal heating, cooling, and wind mixing, *J. Geophys. Res.*, *91*, 8411–8427, 1986.

Ratcliffe, R. A. S., and R. Murray, New lag associations between North Atlantic sea temperature and European pressure applied to long-range weather forecasting, *Q. J. R. Meteorol. Soc.*, *96*, 226–246, 1970.

Smith, P. C., The mean and seasonal circulation off southwest Nova Scotia, *J. Phys. Oceanogr.*, *13*, 1034–1054, 1983.

Smith, P. C., and C. Anderson, Oceanographic observation on the Scotian Shelf during CASP, *Atmos. Ocean*, *27*, 130–156, 1989.

Smith, P. C., and F. B. Schwing, Mean circulation and variability on the eastern Canadian continental shelf, *Cont. Shelf Res.*, *11*, 977–1012, 1991.

Smith, S. D., and F. W. Dobson, The heat budget at ocean weather station Bravo, *Atmos. Ocean*, *22*, 1–22, 1984.

Thompson, K. R., and M. G. Hazen, Interseasonal changes of wind stress and Ekman upwelling: North Atlantic, 1950–1980, *Can. Tech. Rep. Fish. Aquat. Sci.*, *1214*, 175 pp., 1983.

Thompson, K. R., R. H. Loucks, and R. W. Trites, Sea surface temperature variability in the shelf-slope region of the northwest Atlantic, *Atmos. Ocean*, *26*, 282–299, 1988.

Umoh, J. U., Seasonal and interannual variability of sea temperature and surface heat fluxes in the northwest Atlantic, Ph.D. thesis, 237 pp., Dalhousie Univ., Halifax, N. S., Canada, 1992.

Weare, B. C., Empirical orthogonal function analysis of Atlantic Ocean surface temperatures, *Q. J. R. Meteorol. Soc.*, *103*, 467–478, 1977.

Weare, B. C., A. R. Navato, and R. E. Newell, Empirical orthogonal function analysis of Pacific sea surface temperature, *J. Phys. Oceanogr.*, *6*, 671–678, 1976.

K. R. Thompson and J. U. Umoh, Department of Oceanography, Dalhousie University, Halifax, Nova Scotia, Canada B3H 4J1.

(Received August 31, 1993; revised May 4, 1994;
accepted May 13, 1994.)